



HAL
open science

Hygroscopicity of the submicrometer aerosol at the high-alpine site Jungfraujoch, 3580 m a.s.l., Switzerland

S. Sjogren, M. Gysel, E. Weingartner, M. R. Alfarra, J. Duplissy, J. Cozic, J. Crosier, H. Coe, Urs Baltensperger

► To cite this version:

S. Sjogren, M. Gysel, E. Weingartner, M. R. Alfarra, J. Duplissy, et al.. Hygroscopicity of the submicrometer aerosol at the high-alpine site Jungfraujoch, 3580 m a.s.l., Switzerland. *Atmospheric Chemistry and Physics Discussions*, 2007, 7 (5), pp.13699-13732. hal-00303104

HAL Id: hal-00303104

<https://hal.science/hal-00303104>

Submitted on 18 Jun 2008

HAL is a multi-disciplinary open access archive for the deposit and dissemination of scientific research documents, whether they are published or not. The documents may come from teaching and research institutions in France or abroad, or from public or private research centers.

L'archive ouverte pluridisciplinaire **HAL**, est destinée au dépôt et à la diffusion de documents scientifiques de niveau recherche, publiés ou non, émanant des établissements d'enseignement et de recherche français ou étrangers, des laboratoires publics ou privés.

**Hygroscopicity
Jungfraujoch,
Switzerland**

S. Sjogren et al.

Hygroscopicity of the submicrometer aerosol at the high-alpine site Jungfraujoch, 3580 m a.s.l., Switzerland

S. Sjogren¹, M. Gysel¹, E. Weingartner¹, M. R. Alfarra¹, J. Duplissy¹, J. Cozic¹,
J. Crosier², H. Coe², and U. Baltensperger¹

¹Laboratory of Atmospheric Chemistry, Paul Scherrer Institut, 5232 Villigen, Switzerland

²School of Earth, Atmospheric and Environmental Science, University of Manchester, UK

Received: 16 August 2007 – Accepted: 12 September 2007 – Published: 19 September 2007

Correspondence to: E. Weingartner (ernest.weingartner@psi.ch)

Title Page

Abstract

Introduction

Conclusions

References

Tables

Figures

◀

▶

◀

▶

Back

Close

Full Screen / Esc

Printer-friendly Version

Interactive Discussion

Abstract

Data from measurements of hygroscopic growth of submicrometer aerosol with a hygroscopicity tandem differential mobility analyzer (HTDMA) during four campaigns at the high alpine research station Jungfraujoch, Switzerland, are presented. The campaigns took place during the years 2000, 2002, 2004 and 2005, each lasting approximately one month. In parallel, size resolved chemical composition measurements with an aerosol mass spectrometer were performed. A hygroscopic closure was done with the composition data using the Zdanovskii-Stokes-Robinson relation. In general, a good agreement between measured and modeled data was found, with some discrepancies caused by instrumental noise at low aerosol loadings. Hygroscopic growth factors (GF , i.e. the relative change in particle diameter from dry diameter, D_0 , to diameter measured at higher relative humidity, RH) are presented for three distinct air mass types, namely for: 1) free tropospheric winter conditions, 2) planetary boundary layer influenced air masses (during a summer period) and 3) Saharan dust events (SDE). The GF values at 85% RH ($D_0=100$ nm) were 1.40 ± 0.11 and 1.29 ± 0.08 for the first two situations while for SDE a bimodal GF distribution was often found. No phase changes were observed when the RH was varied between 10–90%, and the continuous water uptake could be well described with a single-parameter empirical model. The frequency distributions of the average hygroscopic growth factors and the width of the retrieved growth factor distributions (indicating whether the aerosol is internally or externally mixed) are presented, which can be used for modeling purposes.

1 Introduction

Aerosol particles in the atmosphere affect the earth's radiation balance in various ways (e.g. Solomon et al., 2007). Firstly, aerosol particles absorb and scatter radiation. This direct aerosol effect is influenced by the hygroscopicity of the aerosol particles, which is determined mainly by their chemical composition. Secondly, the tendency for cloud

Hygroscopicity Jungfraujoch, Switzerland

S. Sjogren et al.

Title Page

Abstract

Introduction

Conclusions

References

Tables

Figures

◀

▶

◀

▶

Back

Close

Full Screen / Esc

Printer-friendly Version

Interactive Discussion

**Hygroscopicity
Jungfraujoch,
Switzerland**S. Sjogren et al.

[Title Page](#)[Abstract](#)[Introduction](#)[Conclusions](#)[References](#)[Tables](#)[Figures](#)[◀](#)[▶](#)[◀](#)[▶](#)[Back](#)[Close](#)[Full Screen / Esc](#)[Printer-friendly Version](#)[Interactive Discussion](#)

formation and resulting cloud properties similarly depend on chemical composition as well as on size distribution of the aerosol particles (e.g. McFiggans et al., 2006). Thus the cloud albedo and the radiative properties of cloud droplets are influenced; this is termed the indirect aerosol effect. The presence of particulate water allows for physical processes (e.g., shape modification) or heterogeneous chemical reactions, which in turn influences the chemical composition. These processes are commonly referred to as the ageing of aerosols.

Aerosols and their properties, such as hygroscopicity, are currently modeled in global climate models (GCMs), mostly to better predict the scattering properties and size distribution under varying humidity conditions (Randall et al., 2007). Relatively few measurements of background aerosol from the lower free troposphere exist (e.g. Kandler and Schütz, 2007). To increase available data and validation possibilities four measurement campaigns at the high alpine site Jungfraujoch (JFJ), with a duration of about one month each, are presented here. During 2000, 2002, 2004 and 2005 the CLACE (**CL**oud and **A**erosol **C**haracterization **E**xperiment) field studies were performed within international collaborations, including both summer and winter seasons. The general goals of the field campaigns were i) a physical, chemical, and optical characterization of the aerosol at the JFJ in order to better quantify the direct aerosol effect, and ii) an investigation of the interaction of aerosol with clouds, for a better quantification of the indirect effect. The cloud forming processes were studied under different meteorological conditions, with a special focus on aerosol-cloud partitioning in mixed-phase clouds (Cozic et al., 2007a; Verheggen et al., 2007). Further topics were the physical and chemical characterization of ice nuclei (Cozic et al., 2007b¹; Mertes et al., 2007), and the processes responsible for the formation of new particles in the free troposphere. Instrumentation was deployed to characterize the aerosol size distribution (scanning particle mobility sizer and optical particle counter), size segregated chemical compo-

¹Cozic, J., Mertes, S., Verheggen, B., Cziczo, D. J., Gallavardin, S. J., Baltensperger, U., and Weingartner, E.: Field observation of black carbon enrichment in atmospheric ice particle residuals suggesting a potential ice nucleating capability, submitted, J. Geophys. Res., 2007b.

sition (Aerodyne aerosol mass spectrometer, AMS) and hygroscopicity (hygroscopicity tandem differential mobility analyzer, HTDMA). In this study AMS and HTDMA results will be analyzed in greater detail.

Atmospheric aerosol components can be classified into inorganic and organic fractions (e.g. Kanakidou et al., 2005). The hygroscopic properties of most inorganic salts present in the atmospheric aerosol are known. Of the many organic species identified in the aerosol (e.g. Putaud et al., 2004), the hygroscopic properties of quite a few substances have been investigated. Inorganic salts (for instance ammonium sulfate (AS) and sodium chloride (NaCl) can show a hysteresis behavior during uptake and loss of water, i.e. by exhibiting a difference between the deliquescence and efflorescence relative humidities (DRH/ERH), and with a higher water content of the deliquesced than the effloresced particles in this relative humidity (RH) range. Conversely, organic constituents of the aerosol often do not show efflorescence which can contribute to an uptake of water at lower RH than the DRH of inorganic salts.

A method for characterizing water uptake is the HTDMA (Liu et al., 1978; Rader and McMurry, 1986; Weingartner et al., 2002). The set-up used in three of the campaigns was a low-temperature HTDMA (-10°C during the winter campaigns and 0.5°C during the summer campaign), and in the winter campaign 2005 measurements were done at laboratory temperature ($25\text{--}33^{\circ}\text{C}$). Furthermore, measurements with an AMS supplied time- and mass-resolved chemical composition of sulfate, nitrate, ammonium and organics during the campaigns 2002, 2004 and 2005. The hygroscopic growth was predicted with the Zdanovskii-Stokes-Robinson (ZSR) relation using the measured composition from the AMS (Gysel et al., 2006; Stokes and Robinson, 1966), and compared with the hygroscopicity measured by the HTDMA.

**Hygroscopicity
Jungfraujoch,
Switzerland**S. Sjogren et al.

[Title Page](#)[Abstract](#)[Introduction](#)[Conclusions](#)[References](#)[Tables](#)[Figures](#)[◀](#)[▶](#)[◀](#)[▶](#)[Back](#)[Close](#)[Full Screen / Esc](#)[Printer-friendly Version](#)[Interactive Discussion](#)

2 Methods

2.1 Site and air mass types

The JFJ is a European high-alpine background site located on an exposed mountain col in the Bernese Alps, Switzerland, at 3580 m altitude (46.33° N, 7.59° E). Throughout the year the station is within clouds about one third of the time (Baltensperger et al., 1998). During winter it is predominantly in lower free tropospheric air masses. During summer the aerosol sampled is influenced by injections of air from the planetary boundary layer (PBL) (Baltensperger et al., 1997; Nyeki et al., 2000). The station is surrounded by glaciers and rocks, and no local vegetation is present. The JFJ boasts the highest European (electrical) railway station and is easily accessible throughout the year. Within the World Meteorological Organization (WMO) Global Atmosphere Watch (GAW) program continuous measurements of aerosol parameters have been performed at the JFJ site since 1995 (Collaud Coen et al., 2007). The research station is also part of the Swiss National Monitoring Network for Air Pollution (NABEL) and the Swiss Meteorological Institute (SMI).

The aerosol loading at the JFJ shows an annual cycle with highest concentrations in August to July and minimum concentrations in January to February (e.g. Cozic et al., 2007c; Nyeki et al., 1998; Weingartner et al., 1999). Based on comparison with the continuous aerosol measurements that are available for the JFJ since 1995, campaigns in 2000 and 2004 appear as typical winter conditions (with low aerosol concentration present in the free troposphere), while the campaign in 2002 is typical of summer conditions, and the 2005 campaign can be considered as spring-like conditions, with features situated in between winter and summer. In the following, the data are separated accordingly to these cases: non-disturbed lower free tropospheric winter conditions (abbreviated FT) and PBL influenced summer conditions (abbreviated PBL INF). Further, at times the JFJ is influenced by Saharan dust events (SDE). These events were detected according to the method described by Collaud Coen et al. (2004), which shows that during SDE the Angström exponent of the single scattering albedo

Hygroscopicity Jungfraujoch, Switzerland

S. Sjogren et al.

Title Page

Abstract

Introduction

Conclusions

References

Tables

Figures

◀

▶

◀

▶

Back

Close

Full Screen / Esc

Printer-friendly Version

Interactive Discussion

is negative. This method was also corroborated by size resolved chemical analysis by ion chromatography, where, during dust events, ~6% of the total calcium concentration was found in the PM₁ samples. Thus, a third type of air mass (abbreviated SDE) is distinguished here. The criterion used for SDE was when the Angström exponent was less than -0.1 for more than three hours. Conversely non-disturbed FT air masses were defined as the periods where the Angstrom exponent was positive, and furthermore 1 h around each SDE was removed from the data to avoid transition periods.

2.2 Measurements

Several different inlets were used during the experiments. In this study a heated total inlet (25°C) was used, which was designed to evaporate the condensed water from cloud hydro-meteors thus sampling the sum of all particles including both cloud droplet residual and interstitial particles. Calculations for this setup showed that cloud droplets smaller than 40 μm can be sampled at wind speeds up to 20 m s⁻¹ (Weingartner et al., 1999). An interstitial inlet was operated with a PM₁ or PM_{2.5} cyclone and sampled only the interstitial submicron-sized aerosol, with hydro-meteors being precipitated in the cyclone. The difference in response downstream of the two different inlets provides insight into the fractionation of aerosol particles between the cloud phase and the interstitial phase. Table 1 lists the dates for the campaigns as well as details of instruments used and setup of the HTDMA.

2.3 AMS (Aerosol Mass Spectrometer)

An Aerodyne quadruple AMS (Jayne et al., 2000) was used to provide on-line, quantitative measurements of the total mass and size distributed non refractory chemical composition of the submicron ambient aerosol at a high temporal resolution. The instrument works by sampling air through an aerodynamic lens to form a particle beam in a vacuum and accelerating the focused beam of particles as a function of their momentum towards a tungsten heater (550°C) that flash vaporizes the particles. The

Title Page

Abstract

Introduction

Conclusions

References

Tables

Figures

◀

▶

◀

▶

Back

Close

Full Screen / Esc

Printer-friendly Version

Interactive Discussion

volatilization stage is performed adjacent to an electron impact ionizer (about 70 eV) and the ions are analyzed by a quadruple mass spectrometer (QMA 410, Balzers, Liechtenstein) with unit mass-to-charge (m/z) resolution. In typical field operation, the AMS alternates between two modes: (i) in the mass-spectrum (MS) mode the averaged chemical composition of the non-refractory (NR) aerosol ensemble is determined by scanning the m/z spectrum with the quadruple mass spectrometer, without size resolved information, (ii) using the aerosol time-of-flight (ToF) mode selected m/z representative of key chemical components can be resolved as a function of the vacuum aerodynamic diameter of the particles. More detailed descriptions of the AMS measurement principles and various calibrations (Canagaratna et al., 2007; Jayne et al., 2000), its modes of operation (Jimenez et al., 2003) and data processing and analysis (Allan et al., 2003; Allan et al., 2004) are available. The AMS supplies the concentrations of inorganic ions, i.e. sulfate, nitrate and ammonium. These ions account for 96% of the composition of inorganic ions at the JFJ (Cozic et al., 2007c; Henning et al., 2003; Krivacsy et al., 2001). Furthermore the total concentration of the organic content is supplied, although no detailed speciation is possible. Mass loadings at the JFJ site are generally low. Therefore 3-h averages were calculated as a compromise between counting statistics and time resolution.

2.4 Black carbon concentration

During the first two campaigns 2000 and 2002 the black carbon (BC) concentration was measured with an AE31 Aethalometer (at wavelength $\lambda=880$ nm) (Weingartner et al., 2003). During the last two campaigns BC was measured with a multiple angle absorption photometer (MAAP, at $\lambda=630$ nm) as well as with an AE31 Aethalometer (at $\lambda=880$ nm). A mass absorption efficiency of $7.6 \text{ m}^2 \text{ g}^{-1}$ for winter and $11.1 \text{ m}^2 \text{ g}^{-1}$ for summer was used for the MAAP data (Cozic et al., 2007c). BC concentrations from the aethalometer were determined accordingly, taking advantage of a high correlation between these two instruments during simultaneous measurements (Cozic et al., 2006). As no size resolved BC measurements were available it was assumed that the BC

Title Page

Abstract

Introduction

Conclusions

References

Tables

Figures

◀

▶

◀

▶

Back

Close

Full Screen / Esc

Printer-friendly Version

Interactive Discussion

fraction in each size range was independent of size and thus equal to the BC fraction in PM1 (defined as the sum of the AMS and the BC data). The choice of the mass absorption efficiency for the BC concentration and the assumption of size independence are not critical due to the low sensitivity of the hygroscopicity closure to these values.

5 2.5 HTDMA (Hygroscopicity Tandem Differential Mobility Analyzer)

Briefly, the HTDMA functions as follows: a differential mobility analyzer (DMA1) selects a monodisperse aerosol size cut with mobility diameter, D_0 , under dry conditions. The aerosol then passes through a humidifier with a controlled higher RH, and the mobility diameter D is measured with a second DMA (DMA2). The two DMAs are similar to the TSI 3071 type. The relevant RH in DMA2 was determined by measurement of the system temperature and the DMA2 excess sheath air dew point using a dew point mirror (model 2002 Dewprime, EdgeTech). The accuracy of the RH measurement at higher RH is for example $85 \pm 1.1\%$, assuming no temperature gradients in the DMA2. The residence time of the sampled aerosol at the set RH was >20 s before size measurement (Sjogren et al., 2007). The HTDMAs were employed in slightly different ways during the different campaigns (see Table 1). In general the HTDMA measured at a constant RH which was set to 85%. On occasions the RH-dependence of the hygroscopic growth was investigated by both increasing and decreasing the RH in DMA2 between 10 and 85%. These are known as the dehydration and hydration modes of operation, respectively. This allows for detecting potential hysteresis effects in the hygroscopic growth behavior with distinct efflorescence and deliquescence transitions. The hydration mode, where the mono-modal dry particles were exposed to a monotonically increasing RH in the HTDMA prior to the size measurement in DMA2 (allowing measurements of DRH), was applied during all campaigns, and is also the mode of operation used during measurements at constant RH. The dehydration mode, where the dry particles are first exposed to $RH > 80\%$ using a pre-humidifier before monotonically lowering the RH towards the RH in DMA2 (Gysel et al., 2004; Sjogren et al., 2007), was mainly applied during the 2004 winter campaign (allowing measurements of ERH).

Title Page

Abstract

Introduction

Conclusions

References

Tables

Figures

◀

▶

◀

▶

Back

Close

Full Screen / Esc

Printer-friendly Version

Interactive Discussion

The hygroscopic growth factor (GF) indicates the relative increase in mobility diameter of particles due to water absorption at a certain RH, and is defined as

$$GF(RH) = \frac{D(RH)}{D_0} \quad (1)$$

where $D(RH)$ is the mobility diameter at a specific RH and D_0 is the particle mobility diameter measured under dry conditions (91% of the data were with DMA1 at RH<15%. However to increase available data we included periods where the RH in DMA1 was up to 35%, where the GF is relatively low (<1.03) for the ambient aerosol (see below).

Mobility diameter growth factors obtained with an HTDMA are only equal to volume equivalent growth factors if the particles do not change their shape during water uptake.

This assumption is justified as the hygroscopicity was characterized by a continuous growth curve for the majority of the time (see below), thus the particles can be considered liquid and consequently roughly spherical at all measured RH.

During the first three campaigns both DMAs and the humidifier were inserted in a well-circulated water bath, ensuring constant temperature as indicated. The aerosol line was cooled and insulated from the outside of the building to the entry of the first DMA. This ensured that no artifacts during the sampling occurred (i.e. volatilization of semi-volatile material), as the measurements were performed close to ambient temperatures (Gysel et al., 2002; Weingartner et al., 2002). During the campaign in 2005 the first DMA was maintained at the laboratory temperature (25–33°C) and only DMA2 was kept at a constant temperature in a water bath (22.8°C) (Sjogren et al., 2007). This was done because of the functionality of the HTDMA used, and because it was deduced from the three first campaigns that temperature artifacts were negligible (i.e. compared to measurement uncertainties). The HTDMA data were averaged to 3 h, in order to match the AMS time series. The performance of the instruments was verified with extensive testing with AS and NaCl before the campaigns. During 2004 and 2005 these salts were also measured at the JFJ. The growth of AS and NaCl particles was compared with the theoretical prediction using the Aerosol Diameter-Dependent Equilibrium Model (ADDEM) (Topping et al., 2005a, 2005b), and corresponded to within

Hygroscopicity Jungfraujoch, Switzerland

S. Sjogren et al.

[Title Page](#)[Abstract](#)[Introduction](#)[Conclusions](#)[References](#)[Tables](#)[Figures](#)[◀](#)[▶](#)[◀](#)[▶](#)[Back](#)[Close](#)[Full Screen / Esc](#)[Printer-friendly Version](#)[Interactive Discussion](#)

less than 0.04 in GF at 85% RH.

2.5.1 Inversion algorithm

Atmospheric particles of a defined dry size typically exhibit a range of growth factors or even clearly separated growth modes, because of external mixing or variable relative fractions of different compounds in individual particles (hereinafter referred to as quasi-internally mixed). Growth factor probability distributions $c(GF)=dC/dGF$ are retrieved from each measurement, and normalized such that $C = \int c(GF)dGF = 1$. The inversion method applied to the raw data (Gysel et al., 2007²) has similarities to the inversion algorithm described by Cubison et al. (2005). The distribution $c(GF)$ is also inverted from the measurement distribution into contributions from fixed classes of narrow growth factor ranges, but instead of using a linear inversion, $c(GF)$ is fitted to the actual measurements using a full TDMA transfer forward model. A bin resolution of $\Delta GF=0.15$ was chosen for the inversion because of counting statistics.

The AMS provides chemical composition data for the entire submicron aerosol particle ensemble in the air sample, whereas no information on the mixing state of individual particles is obtained. Inverted growth factor distributions $c(GF)$ obtained with the HTDMA provide some information on the mixing state. The ensemble mean growth factor GF^* is defined as the 3rd-moment mean growth factor of $c(GF)$. GF^* represents the growth factor that would be observed if the absorbed water were equally distributed among all particles, even in the case of several distinct growth modes. Thus GF^* is the quantity to be compared with growth factor predictions based on composition data obtained by the AMS (see below). Thus even if the measured GF is broad or even clearly bimodal GF^* would represent the hygroscopicity as predicted from the AMS data as long as the AMS can measure all the relevant chemical components in both modes. This is not the case if some of the material sampled is composed of a refractory component such as dust, black carbon or sea salt that cannot be observed by the

²Gysel, M., McFiggans, G. B., Coe, H., et al.: Inversion of TDMA data, in preparation, 2007.

Title Page

Abstract

Introduction

Conclusions

References

Tables

Figures

⏪

⏩

◀

▶

Back

Close

Full Screen / Esc

Printer-friendly Version

Interactive Discussion

AMS.

The standard deviation σ of the inverted growth factor distribution $c(GF)$ is used as a measure for the spread of growth factors. With a bin resolution of $\Delta GF=0.15$ as chosen here for the HTDMA data inversion, the σ that would be obtained for a perfectly internally mixed aerosol with a well defined growth factor (i.e. $\sigma=0$) is between 0.06 and 0.10 depending on the bin positions relative to the GF^* . The σ obtained with pure ammonium sulfate at 85% RH is <0.05 , when inverting the data with high resolution. Therefore any $\sigma \leq 0.10$ indicates absence of distinct growth modes, i.e. a quasi-internal mixture with limited spread of growth factors, while any $\sigma \geq 0.15$ shows that the aerosol is externally mixed or quasi-internally mixed with substantial spread of growth factors. We use the σ not only to describe the spread of a single mode, but also in the sense of describing a broader distribution, or describing cases which are clearly bimodal. Two HTDMA measurement examples (red) and corresponding inverted growth factor distributions (green) as well as the inverted growth distribution reprocessed through the HTDMA forward model (blue) are shown in Fig. 1. Panel (A) shows an aerosol ($D_o=100$ nm) observed during undisturbed FT conditions with $GF^*=1.28$ and $\sigma=0.08$, indicating that it was internally mixed. Panel (B) shows an aerosol observed during an SDE with $\sigma=0.22$. This aerosol is obviously externally mixed with two distinct modes at $GF=1.05$ and $GF=1.45$, whereof the former can be attributed to mineral dust. The GF^* is 1.227 and is not representative of the hygroscopic behavior of the aerosol but would be the value to compare with the predicted hygroscopicity from the ensemble chemical composition, which would need to take mineral dust into account. In this case the blue line does not exactly follow the measurement because of the limited resolution of the inversion. However, better results cannot be obtained even with increasing the resolution, because the measurement uncertainties are too big at such a low number of measured counts.

Title Page

Abstract

Introduction

Conclusions

References

Tables

Figures

◀

▶

◀

▶

Back

Close

Full Screen / Esc

Printer-friendly Version

Interactive Discussion

2.5.2 Correction of HTDMA data to 85% RH

The measurements were generally done at 85% RH. To obtain a more complete time series data set, data between 80 and 90% RH were corrected to 85% RH using the following equation:

$$k(GF, a_w) = \frac{(GF^3 - 1)(1 - a_w)}{a_w} \Leftrightarrow GF_{RH=85\%}(a_w, k) = \left(1 + k \frac{a_w}{1 - a_w}\right)^{1/3} \quad (2)$$

where k captures all solute properties. a_w is the water activity. First the k -value was calculated from the measured GF and RH (left hand side of Eq. 2), and then the corresponding corrected GF at 85% was calculated using this k (right hand side of Eq. (2)). Equation (2) is equivalent to Eq. (4) in the paper by Gysel et al. (2004) with $k = (M_w \rho_s i_s) / (\rho_w M_s)$, where M_w is the molar mass and ρ_w the density of water, and M_s the molar mass, ρ_s the density and i_s the van't Hoff factor of the solute. Equation (2) is also equivalent to Eq. (1) in the paper by Dick et al. (2000) with $a = k$ and $b = c = 0$, where a , b , and c are their model parameters. More details about the theoretical background of the functionality of Eq. (2) are given in Kreidenweis et al. (2005). Using a constant k -value for RH corrections is equivalent to a constant van't Hoff factor. This assumption is justified for differences of $\pm 5\%$ RH as chosen here.

2.6 ZSR relation

The hygroscopic growth factor of a mixture (GF_{mixed}) can be estimated from the growth factors of the individual components of the aerosol and their respective volume fractions, ε , with the ZSR relation (Gysel et al., 2004; Stokes et al., 1966):

$$GF_{\text{mixed}} = \left(\sum_k \varepsilon_k GF_k^3 \right)^{1/3} \quad (3)$$

where the summation is performed over all compounds present in the particles. The model assumes that: the particles are spherical; ideal mixing behavior (i.e. no volume

Title Page

Abstract

Introduction

Conclusions

References

Tables

Figures

◀

▶

◀

▶

Back

Close

Full Screen / Esc

Printer-friendly Version

Interactive Discussion

change upon mixing); and independent water uptake of the organic and inorganic components. The volume fractions ϵ_i or the components in the particles were calculated as

$$\epsilon_i = \frac{(w_i/\rho_i)}{\sum_k (w_k/\rho_k)} \quad (4)$$

5 where w_i is the measured mass fraction and ρ_i the density of component i .

The AMS measured size-resolved component mass concentrations during the last three campaigns: 2002, 2004 and 2005. We compared the fraction of particles in the range 88–196 nm vacuum aerodynamic diameter (d_{va}) from the AMS with the measured 100 nm mobility diameter (d_{mob}) from the HTDMA. The range was chosen so
10 that the volume difference was equal on each side of 100 nm, (i.e. 49–122 nm in d_{mob}). The chosen width of the size range is a compromise between size resolution and signal statistics. The mobility diameter can be calculated from the aerodynamic diameter as follows (Zelenyuk et al., 2006), with the assumption that the particles are spherical ($\chi_v=1$, dynamic shape factor in the free molecular regime):

$$15 \quad d_{mob} = \frac{\rho_0 d_{va}}{\rho_p \chi_v} \quad (5)$$

Where ρ_0 is standard density (1000 kg m^{-3}) and ρ_p is the particle density. The particle density was calculated from the bulk composition averaged over the campaigns and was 1565 kg m^{-3} . In general the hygroscopicity, predicted with ZSR relation, is more sensitive to substances with higher GF than the ones closer to 1.0 due to the cubic weighting. Thus it is more important to accurately predict the hygroscopicity of the
20 pure inorganic salts, than the organic or the soot components. A second factor of importance is the correct determination of the volume fractions of the more hygroscopic substances. All individual growth factors and densities used were taken from literature (see Table 2).

Hygroscopicity Jungfraujoch, Switzerland

S. Sjogren et al.

[Title Page](#)[Abstract](#)[Introduction](#)[Conclusions](#)[References](#)[Tables](#)[Figures](#)[◀](#)[▶](#)[◀](#)[▶](#)[Back](#)[Close](#)[Full Screen / Esc](#)[Printer-friendly Version](#)[Interactive Discussion](#)

2.7 Neutralization of aerosol

If one considers the major ions present in the JFJ PM₁ aerosol, and the ones with concentrations available from the AMS and filters, namely SO₄²⁻, NO₃⁻, NH₄⁺, the aerosol mixture was mostly neutralized (Cozic et al., 2007c). However, occasionally the measured ammonium concentration was insufficient to fully neutralize the sulfuric acid, indicating an acidic aerosol. Then it was assumed that an equilibrium with first NH₄HSO₄ and subsequently H₂SO₄ was formed. As expected during cases with incomplete neutralization the NO₃⁻ values were low. Note that this choice of sulfate salts is crucial for a correct application of the ZSR mixing rule, i.e. choosing only a combination of H₂SO₄ and (NH₄)₂SO₄ to match the measured sulfate and ammonium concentrations would result in significant prediction errors (Gysel et al., 2006). Splitting the sulfate salts based on the measured ammonium may not be highly accurate, but it indicates at least whether the aerosol is neutralized or acidic. The mass fractions of the different components are shown in the time series in Fig. 4.

3 Results

3.1 Hygroscopicity at the JFJ

The RH-dependence of *GF* was measured by variation of the RH in the HTDMA between 10 and 85%. Figure 2 shows three typical humidograms examples showing the features observed at the JFJ. Generally a continuous growth without differences between hydration and dehydration operating mode was found, thus indicating absence of phase changes. This does not exclude existence of efflorescence at RH < 10%, because our measurements were technically limited to RH > ~10%. Such continuous growth is expected and has been reported for complex mixtures with an increasing number of organic components (Marcolli et al., 2004; Marcolli and Krieger, 2006). The aerosol at the JFJ seems to exist predominantly as dissolved liquid or amorphous par-

Title Page

Abstract

Introduction

Conclusions

References

Tables

Figures

◀

▶

◀

▶

Back

Close

Full Screen / Esc

Printer-friendly Version

Interactive Discussion

5 ticles. Furthermore, the growth curves can be well described with the single-parameter (k) semi-empirical model given in Eq. (2), as can be seen from the solid lines in Fig. 2. The growth curves were also fitted with an empirical power law fit $GF=(1-a_w)^Y$ (Swietlicki et al., 2000), dashed lines in Fig. 2, but for this model we found consistently larger χ^2 -residuals than with the former model. As can be seen from Figs. 2, 3 and 4 the magnitude of the hygroscopic growth at the JFJ varies substantially over time, but the RH-dependence at any time can be captured with a single parameter (k).

10 Figure 3 shows the temporal evolution of GF distributions for a period of the campaign in 2000. Several SDE were observed, as indicated with the shaded areas in Panel (A). During undisturbed FT conditions, a size dependence of the growth factor can be seen, with larger growth for larger particles. This feature, which has previously been shown by Weingartner et al. (2002), was also observed during the other campaigns and is attributed to a size dependent chemical composition. This is confirmed by larger k -values at larger dry diameters (top panel of Fig. 3), which are a measure of the hygroscopicity without the influence of the Kelvin effect. The ensemble k -values have been calculated from the ensemble mean growth factor GF^* using Eq. (2), whereas the water activity corresponding to the measured RH has been calculated assuming a surface tension of pure water. It is hypothesized that smaller particles contain a larger fraction of organic compounds from secondary organic aerosol (SOA) formation. Such a dependence was confirmed by AMS measurements during summer 2002 (Alfarra, 2004). During major SDE two distinct growth modes can be seen for the 250 nm particles, while no clear change in hygroscopic behavior is seen for the 50 nm particles. This is also reflected in strongly decreasing k -values at $D_0=250$ nm, while little or no changes occur at $D_0=100$ and 50 nm. Thus mineral dust particles are only found at larger sizes. As during SDE larger sized particles are more externally mixed, the reduction of the k -value in these periods only reflects the influence of the increasing amount of particles, presumably mineral dust, with lower hygroscopicity, not the k -value of each mode.

25 In summer, a strong diurnal variation is typically found in most aerosol variables (Lu-

**Hygroscopicity
Jungfraujoch,
Switzerland**S. Sjogren et al.

Title Page

Abstract

Introduction

Conclusions

References

Tables

Figures

◀

▶

◀

▶

Back

Close

Full Screen / Esc

Printer-friendly Version

Interactive Discussion

gauer et al., 2000). During the 2002 campaign this diurnal variation was also present in the observed mass loadings, though to a slightly lesser extent (Alfarra, 2004). However, the mass fractions of different components did not vary to a large degree during this diurnal variation, resulting in a fairly constant hygroscopicity on a timescale of hours seen both in the HTDMA results and in the closure (Fig. 4). However, more data with days showing a strong diurnal variation are required for a conclusive description of this influence. As can be seen from the GF^* values in Table 3, the summer campaign is characterized by lower hygroscopicity, due to a higher organic loading (68% in summer compared to 42% in winter). This is most probably due to higher emission rates of SOA precursors and higher photo-oxidation activity, which can also be transported upwards through valley venting.

Figure 4 shows the predicted growth and GF^* for the campaigns 2002, 2004 and 2005 (no high time resolution composition data were available for 2000). A growth factor for organic compounds of 1.2 at $a_w=0.85$, corresponding to 1.182 for a 100 nm particle at 85% RH was used in this work, which is in agreement with smog chamber experiments of organic aerosols (Duplissy et al., 2007³; Baltensperger et al., 2005). The sensitivity to this value was tested by comparing the model fit to the data over several values of GF_{org} and 1.2 at $a_w=0.85$ gave the best fit with a slope of 1, though the fit is relatively insensitive as the influence of GF_{org} is relatively low compared to the influence of the inorganic fraction. The mass spectrum delivered by the AMS at the Jungfraujoch is characterized by a relatively low m/z 57 signal indicating that little unprocessed primary organic material is present and that the majority of the organics are composed of oxidized organic mater (Alfarra et al., 2006; Zhang et al., 2007). During SDE there will be an increased fraction of mostly insoluble mineral dust material (Vlasenko et al., 2006) which is not detected in the AMS. This will lead to an increase

³Duplissy, J., Gysel, M., Alfarra, M. R., Dommen, J., Metzger, A., Prevot, A. S. H., Weingartner, E., Laaksonen, A., Raatikainen, T., Good, N., Turner, S. F., McFiggans, G., and Baltensperger, U.: The cloud forming potential of secondary organic aerosol under near atmospheric conditions, *Geophys. Res. Lett.*, submitted, 2007.

Hygroscopicity Jungfraujoch, Switzerland

S. Sjogren et al.

Title Page

Abstract

Introduction

Conclusions

References

Tables

Figures

◀

▶

◀

▶

Back

Close

Full Screen / Esc

Printer-friendly Version

Interactive Discussion

in the predicted GF compared to the measured one. However, during 2004 some SDE were detected when both instruments were in operation, but the residuals from measured minus predicted hygroscopicity for these SDE were similar to FT conditions. Probably the mass fraction of mineral dust components were not sufficiently high in the sizes <250 nm to significantly influence the ensemble mean growth factor GF^* .

Recently, Gysel et al. (2006) have found significant discrepancies between measured and predicted GF s if substantial mass fractions of ammonium nitrate were present. They concluded that the most likely cause for the discrepancies was an evaporation artifact of ammonium nitrate in the HTDMA, which was operated at $\sim 25^\circ\text{C}$ and with a residence time of ~ 60 s. No systematic prediction bias for data points with high ammonium nitrate mass fraction was found in the data set presented here. An important difference is that the HTDMA measurements of this study were mostly done at low temperatures ($T = -10$ to 0.5°C) and the residence time was kept short (in the order of 20 s), thus minimizing potential evaporation artifacts.

3.2 Frequency distributions of GF^* and σ

Panels (A), (D) and (G) of Fig. 5 show the averages of the normalized measured GF distributions for each dry size studied and for each air mass category. The air mass types distinguished in this analysis are the SDE, the non-disturbed FT conditions as well as the cases influenced by injections from planetary boundary layer air (i.e., during summer, PBL INF). These averaged growth distributions illustrate the mean number fraction of particles in a defined air mass type exhibiting a certain growth factor, unlike Fig. 1 which shows snapshot growth distributions for a specific time. Thus the averages do not necessarily indicate the mixing state of the aerosol as the temporal variability increases the spread. Most of the time at the JFJ one expects to encounter non-disturbed FT conditions or PBL INF during summer. It has been shown in Collaud Coen et al. (2004) that SDE are present only 5% of the time (yearly average). For the FT conditions the 50 and 100 nm particles appear internally mixed, however with a small fraction of particles with a GF between 1.0–1.2, which is not easily resolved

Title Page

Abstract

Introduction

Conclusions

References

Tables

Figures

◀

▶

◀

▶

Back

Close

Full Screen / Esc

Printer-friendly Version

Interactive Discussion

**Hygroscopicity
Jungfraujoch,
Switzerland**

S. Sjogren et al.

Title Page

Abstract

Introduction

Conclusions

References

Tables

Figures

◀

▶

◀

▶

Back

Close

Full Screen / Esc

Printer-friendly Version

Interactive Discussion

with the inversion considering the instrument limits and the low mass loading. For the 50 nm particles this shoulder at low GF s is less pronounced, but this is to some extent a consequence of the smaller hygroscopicity of the main mode, which is slightly overlapping with this shoulder. Kandler and Schütz (2007) also reported GF values for March 2000 at the JFJ (measured at 90% RH at $\sim 20^\circ\text{C}$), which are in agreement with the GF s shown here. Kandler and Schütz (2007) indicated a bimodal distribution for all sizes, however they do not show the relative number fractions in each mode, which, if small for the lower GF mode, would be in agreement with our data. The PBL INF measurements show a more homogeneous GF distribution, but the hygroscopicity is also lower. SDE only occurred during the two winter campaigns, and for these cases the $D_0=250$ nm particles showed an increase of non-hygroscopic particles in a distinct mode with a GF of 1.0. The hygroscopic properties of the $D_0=50$ and 100 nm particles do not differ between SDE/FT. Panels (B), (E), and (H) of Fig. 5 show the frequency distribution of GF^* , from which the mean GF^* presented in Table 3 has been calculated. The hygroscopicity for summer indicates a similar chemical composition for different sizes, while during winter the hygroscopicity increases with size.

Panels C, F and I of Fig. 5 show the frequency distribution of σ averaged for each of the relevant periods. The σ of individual scans can be used to distinguish between quasi-internally mixed aerosols with limited growth factor spread ($\sigma \leq 0.1$) and externally or quasi-internally mixed aerosols with substantial spread ($\sigma \geq 0.15$). The frequency distribution of σ thus indicates the fraction of time of each period that a certain mixing state (σ) is encountered. The most frequent spread observed in summer is $\sigma = \sim 0.125$ which is internally mixed, whereas larger spread is seen in winter FT conditions. This can be attributed to a larger separation of the main growth mode from the minor fraction of particles with growth factors < 1.2 . For the same reason the spread also increases with particle size in winter with $\sigma = \sim 0.1$, 0.125 and 0.15 for $D_0=50$, 100 and 250 nm particles, respectively. This indicates that even under FT conditions observed during winter the aerosol contains a fraction of particles which appear to remain less processed and thus less hygroscopic also at a remote location. The mineral dust during

SDE mostly influences the larger particles with $D_0=250$ nm, as already exemplified in Figs. 3 and 5A. Here it has to be stressed that different scenarios can end up with a bimodal shape of the mean GF distributions as shown in Fig. 5A. Either the GF distribution is always bimodal with similar number fractions of particles in both modes, or only monomodal but the GF distribution are observed with the mode centered at $GF=\sim 1.0$ or $GF=\sim 1.45$ during 50% of the time each. Frequent occurrence of $\sigma \geq 0.2$ and $GF^*=1.3-1.5$ for $D_0=250$ nm during SDE indicates that the former alternative with simultaneous presence of non-hygroscopic mineral dust and more hygroscopic background particles, both in comparable number fractions, dominates. No clear influence of SDE on σ and GF^* is seen at 50 and 100 nm confirming the finding from Panels (D) and (G).

The frequency distributions of the GF^* and σ can be used to simulate internally or quasi-internally mixed hygroscopic behavior of particles in different air masses encountered at the JFJ. Additionally to the frequency distributions it has to be known whether GF^* and σ are dependent on each other. We explored the relationship between the two distributions, but no dependence between GF^* and σ was found. This is different from results found by Aklilu and Mozurkewich (2004) in the Lower Fraser Valley, British Columbia, who reported a horseshoe-shaped relationship with maximum σ values at intermediate GF .

4 Conclusions

A statistical analysis of measurements from four field campaigns of about one month each at the high alpine site Jungfrauoch is presented. During the winter season when the station was in the undisturbed free troposphere, the average GF measured with an HTDMA was 1.40 ± 0.11 at 85% RH for $D_0=100$ nm particles. During the summer season, due to higher SOA formation, the GF was 1.29 ± 0.08 at 85% RH. During mineral dust events GF distributions were partly bimodal for $D_0=250$ nm particles. The frequency distributions of the width of the retrieved growth factor (internally/externally

Title Page

Abstract

Introduction

Conclusions

References

Tables

Figures

◀

▶

◀

▶

Back

Close

Full Screen / Esc

Printer-friendly Version

Interactive Discussion

mixed) distributions are presented, which can be used for comparison with simulations of the hygroscopic behavior of the aerosol encountered at the JFJ. The hygroscopicity was also predicted using the ZSR mixing rule along with chemical composition data. The ZSR mixing model can be used to predict the variability of measured hygroscopicity of submicrometer particles. However, due to low loadings at the JFJ (apart from times when influenced by PBL), the spread in error of the predicted GF from the chemical composition as well as the error for the HTDMA measurement is on average ± 0.1 , which makes it difficult to verify the absolute hygroscopicity values. The most important factor for the modeling is the accuracy in GF s of the inorganics and their composition. It is also important to consider the separation of SO_4^{2-} into ammonium sulfate, ammonium bisulfate and sulfuric acid.

Acknowledgements. This work was supported by the Swiss National Science Foundation Switzerland (grant no 200021-100280), MeteoSwiss in the framework of the Global Atmosphere Watch Program as well as the EC project ACCENT. The UMan measurements were supported by the UK Natural Environment Research Council. We thank the International Foundation High Altitude Research Stations Jungfraujoch and Gornergrat (HFSJG), who made it possible for us to carry out our experiments at the High Altitude Research Station at Jungfraujoch, and also the caretakers at the station.

References

- Aklilu, Y. A. and Mozurkewich, M.: Determination of external and internal mixing of organic and inorganic aerosol components from hygroscopic properties of submicrometer particles during a field study in the Lower Fraser Valley, *Aerosol Sci. Technol.*, 38(2), 140–154, 2004.
- Alfarra, M. R., Paulsen, D., Gysel, M., Garforth, A. A., Dommen, J., Prevot, A. S. H., Worsnop, D. R., Baltensperger, U., and Coe, H.: A mass spectrometric study of secondary organic aerosols formed from the photooxidation of anthropogenic and biogenic precursors in a reaction chamber, *Atmos. Chem. Phys.*, 6, 5279–5293, 2006, <http://www.atmos-chem-phys.net/6/5279/2006/>.
- Allan, J. D., Jimenez, J. L., Williams, P. I., Alfarra, M. R., Bower, K. N., Jayne, J. T., Coe, H.,

Hygroscopicity Jungfraujoch, Switzerland

S. Sjogren et al.

Title Page

Abstract

Introduction

Conclusions

References

Tables

Figures

◀

▶

◀

▶

Back

Close

Full Screen / Esc

Printer-friendly Version

Interactive Discussion

and Worsnop, D. R.: Quantitative sampling using an Aerodyne aerosol mass spectrometer: 1. Techniques of data interpretation and error analysis, *J. Geophys. Res.*, 108, D3, 4090, doi:10.1029/2002JD002358, 2003.

Allan, J. D., Delia, A. E., Coe, H., Bower, K. N., Alfarra, M. R., Jimenez, J. L., Middlebrook, A. M., Drewnick, F., Onasch, T. B., Canagaratna, M. R., Jayne, J. T., and Worsnop, D. R.: A generalised method for the extraction of chemically resolved mass spectra from Aerodyne aerosol mass spectrometer data, *J. Aerosol Sci.*, 35, 7, 909–922, 2004.

Baltensperger, U., Gäggeler, H. W., Jost, D. T., Lugauer, M., Schwikowski, M., Weingartner, E., and Seibert, P.: Aerosol climatology at the high-alpine site Jungfraujoch, Switzerland, *J. Geophys. Res.*, 102, (D16), 19707–19715, 1997.

Baltensperger, U., Schwikowski, M., Jost, D. T., Nyeki, S., Gäggeler, H. W., and Poulida, O.: Scavenging of atmospheric constituents in mixed phase clouds at the high-alpine site Jungfraujoch part I: Basic concept and aerosol scavenging by clouds, *Atmos. Environ.*, 32(23), 3975–3983, 1998.

Baltensperger, U., Kalberer, M., Dommen, J., Paulsen, D., Alfarra, M. R., Coe, H., Fisseha, R., Gascho, A., Gysel, M., Nyeki, S., Sax, M., Steinbacher, M., Prevot, A. S. H., Sjogren, S., Weingartner, E., and Zenobi, R.: Secondary organic aerosols from anthropogenic and biogenic precursors, *Faraday Discussions*, 130, 265–278, 2005.

Canagaratna, M. R., Jayne, J. T., Jimenez, J. L., Allan, J. D., Alfarra, M. R., Zhang, Q., Onasch, T. B., Drewnick, F., Coe, H., Middlebrook, A., Delia, A., Williams, L. R., Trimborn, A. M., Northway, M. J., DeCarlo, P. F., Kolb, C. E., Davidovits, P., and Worsnop, D. R.: Chemical and microphysical characterization of ambient aerosols with the Aerodyne aerosol mass spectrometer, *Mass Spectrometry Reviews*, 26(2), 185–222, 2007.

Collaud Coen, M. C., Weingartner, E., Schaub, D., Hüglin, C., Corrigan, C., Henning, S., Schwikowski, M., and Baltensperger, U.: Saharan dust events at the Jungfraujoch: detection by wavelength dependence of the single scattering albedo and first climatology analysis, *Atmos. Chem. Phys.*, 4, 2465–2480, 2004, <http://www.atmos-chem-phys.net/4/2465/2004/>.

Collaud Coen, M., Weingartner, E., Nyeki, S., Cozic, J., Henning, S., Verheggen, B., Gehrig, R., and Baltensperger, U.: Long-term trend analysis of aerosol variables at the high alpine site Jungfraujoch, *J. Geophys. Res.*, 112, doi: 10.1029/2006JD007995, 2007.

Cozic, J., Verheggen, B., Mertes, S., Connolly, P., Bower, K., Petzold, A., Baltensperger, U., and Weingartner, E.: Scavenging of black carbon in mixed phase clouds at the high alpine site Jungfraujoch, *Atmos. Chem. Phys. Discuss.*, 6, 11877–11912, 2006,

Hygroscopicity Jungfraujoch, Switzerland

S. Sjogren et al.

Title Page

Abstract

Introduction

Conclusions

References

Tables

Figures

◀

▶

◀

▶

Back

Close

Full Screen / Esc

Printer-friendly Version

Interactive Discussion

<http://www.atmos-chem-phys-discuss.net/6/11877/2006/>.

Cozic, J., Verheggen, B., Mertes, S., Connolly, P., Bower, K., Petzold, A., Baltensperger, U., and Weingartner, E.: Scavenging of black carbon in mixed phase clouds at the high alpine site Jungfrauoch, *Atmos. Chem. Phys.*, 7, (7), 1797–1807, 2007a.

5 Cozic, J., Verheggen, B., Weingartner, E., Crosier, J., Bower, K., Flynn, M., Coe, H., Henning, S., Steinbacher, M., Collaud Coen, M., Petzold, A., and Baltensperger, U.: Chemical composition of free tropospheric aerosol for PM1 and coarse mode at the high alpine site Jungfrauoch, *Atmos. Chem. Phys. Discuss.*, 7, 12 145–12 184, 2007c.

10 Cubison, M. J., Coe, H., and Gysel, M.: A modified hygroscopic tandem DMA and a data retrieval method based on optimal estimation, *J. Aerosol Sci.*, 36(7), 846–865, 2005.

Dick, W. D., Saxena, P., and McMurry, P. H.: Estimation of water uptake by organic compounds in submicron aerosols measured during the Southeastern Aerosol and Visibility Study, *J. Geophys. Res.*, 105, (D1), 1471–1479, 2000.

15 Dinar, E., Mentel, T. F., and Rudich, Y.: The density of humic acids and humic like substances (HULIS) from fresh and aged wood burning and pollution aerosol particles, *Atmos. Chem. Phys.*, 6, 5213–5224, 2006, <http://www.atmos-chem-phys.net/6/5213/2006/>.

Gysel, M., Weingartner, E., and Baltensperger, U.: Hygroscopicity of aerosol particles at low temperatures. 2. Theoretical and experimental hygroscopic properties of laboratory generated aerosols, *Environ. Sci. Technol.*, 36, (1), 63–68, 2002.

20 Gysel, M., Weingartner, E., Nyeki, S., Paulsen, D., Baltensperger, U., Galambos, I., and Kiss, G.: Hygroscopic properties of water-soluble matter and humic-like organics in atmospheric fine aerosol, *Atmos. Chem. Phys.*, 4, 35–50, 2004, <http://www.atmos-chem-phys.net/4/35/2004/>.

25 Gysel, M., Crosier, J., Topping, D. O., Whitehead, J. D., Bower, K. N., Cubison, M. J., Williams, P. I., Flynn, M. J., McFiggans, G. B., and Coe, H.: Closure between measured and modelled particle hygroscopic growth during TORCH2 implies ammonium nitrate artefact in the HTDMA measurements, *Atmos. Chem. Phys. Discuss.*, 6, 12 503–12 548, 2006.

30 Henning, S., Weingartner, E., Schwikowski, M., Gäggeler, H. W., Gehrig, R., Hinz, K. P., Trimborn, A., Spengler, B., and Baltensperger, U.: Seasonal variation of water-soluble ions of the aerosol at the high-alpine site Jungfrauoch (3580 m a.s.l.), *J. Geophys. Res.*, 108, (D1), 2003.

Jayne, J. T., Leard, D. C., Zhang, X. F., Davidovits, P., Smith, K. A., Kolb, C. E., and Worsnop, D. R.: Development of an aerosol mass spectrometer for size and composition analysis of

ACPD

7, 13699–13732, 2007

Hygroscopicity Jungfrauoch, Switzerland

S. Sjogren et al.

Title Page

Abstract

Introduction

Conclusions

References

Tables

Figures

◀

▶

◀

▶

Back

Close

Full Screen / Esc

Printer-friendly Version

Interactive Discussion

EGU

- submicron particles, *Aerosol Sci. Technol.*, 33(1–2), 49–70, 2000.
- Jimenez, J. L., Jayne, J. T., Shi, Q., Kolb, C. E., Worsnop, D. R., Yourshaw, I., Seinfeld, J. H., Flagan, R. C., Zhang, X. F., Smith, K. A., Morris, J. W., and Davidovits, P.: Ambient aerosol sampling using the Aerodyne Aerosol Mass Spectrometer, *J. Geophys. Res.*, 108, (D7), 2003.
- 5 Kanakidou, M., Seinfeld, J. H., Pandis, S. N., Barnes, I., Dentener, F. J., Facchini, M. C., Van Dingenen, R., Ervens, B., Nenes, A., Nielsen, C. J., Swietlicki, E., Putaud, J. P., Balkanski, Y., Fuzzi, S., Horth, J., Moortgat, G. K., Winterhalter, R., Myhre, C. E. L., Tsigaridis, K., Vignati, E., Stephanou, E. G., and Wilson, J.: Organic aerosol and global climate modelling: a review, *Atmos. Chem. Phys.*, 5, 1053–1123, 2005,
<http://www.atmos-chem-phys.net/5/1053/2005/>.
- 10 Kandler, K., and Schütz, L.: Climatology of the average water-soluble volume fraction of atmospheric aerosol, *Atmos. Res.*, 83(1), 77–92, 2007.
- Kreidenweis, S. M., Koehler, K., DeMott, P. J., Prenni, A. J., Carrico, C., and Ervens, B.: Water activity and activation diameters from hygroscopicity data - Part I: Theory and application to inorganic salts, *Atmos. Chem. Phys.*, 5, 1357–1370, 2005,
<http://www.atmos-chem-phys.net/5/1357/2005/>.
- 15 Krivacsy, Z., Gelencser, A., Kiss, G., Meszaros, E., Molnar, A., Hoffer, A., Meszaros, T., Sarvari, Z., Temesi, D., Varga, B., Baltensperger, U., Nyeki, S., and Weingartner, E.: Study on the chemical character of water soluble organic compounds in fine atmospheric aerosol at the Jungfraujoch, *J. Atmos. Chem.*, 39, (3), 235–259, 2001.
- 20 Liu, B. Y. H., Pui, D. Y. H., Whitby, K. T., Kittelson, D. B., Kousaka, Y., and McKenzie, R. L.: The Aerosol Mobility Chromatograph: a new detector for sulfuric acid aerosols, *Atmos. Env.*, 12, 99–104, 1978.
- 25 Lugauer, M., Baltensperger, U., Furger, M., Gäggeler, H. W., Jost, D. T., Nyeki, S., and Schwikowski, M.: Influences of vertical transport and scavenging on aerosol particle surface area and radon decay product concentrations at the Jungfraujoch (3454 m above sea level), *J. Geophys. Res.*, 105, (D15), 19 869–19 879, 2000.
- Marcolli, C., Luo, B. P., and Peter, T.: Mixing of the organic aerosol fractions: Liquids as the thermodynamically stable phases, *J. Phys. Chem.*, 108(12), 2216–2224, 2004.
- 30 Marcolli, C. and Krieger, U. K.: Phase changes during hygroscopic cycles of mixed organic/inorganic model systems of tropospheric aerosols, *J. Phys. Chem.*, 110(5), 1881–1893, 2006.

**Hygroscopicity
Jungfraujoch,
Switzerland**S. Sjogren et al.

Title Page

Abstract

Introduction

Conclusions

References

Tables

Figures

◀

▶

◀

▶

Back

Close

Full Screen / Esc

Printer-friendly Version

Interactive Discussion

McFiggans, G., Artaxo, P., Baltensperger, U., Coe, H., Facchini, M. C., Feingold, G., Fuzzi, S., Gysel, M., Laaksonen, A., Lohmann, U., Mentel, T. F., Murphy, D. M., O'Dowd, C. D., Snider, J. R., and Weingartner, E.: The effect of physical and chemical aerosol properties on warm cloud droplet activation, *Atmos. Chem. Phys.*, 6, 2593–2649, 2006,

<http://www.atmos-chem-phys.net/6/2593/2006/>.

Mertes, S., Verheggen, B., Walter, S., Ebert, M., Connolly, P., Weingartner, E., Schneider, J., Bower, K. N., Inerle-Hof, M., Cozic, J., Baltensperger, U., and Heintzenberg, J.: Counterflow virtual impactor based collection of small ice particles in mixed-phase clouds for the physico-chemical characterisation of tropospheric ice nuclei: sampler description and first case study, *Aerosol Sci. Technol.*, 41(9), 848–864, 2007.

Nyeki, S., Li, F., Weingartner, E., Streit, N., Colbeck, I., Gäggeler, H. W., and Baltensperger, U.: The background aerosol size distribution in the free troposphere: An analysis of the annual cycle at a high-alpine site, *J. Geophys. Res.*, 103, (D24), 31 749–31 761, 1998.

Nyeki, S., Kalberer, M., Colbeck, I., De Wekker, S., Furger, M., Gäggeler, H. W., Kossmann, M., Lugauer, M., Steyn, D., Weingartner, E., Wirth, M., and Baltensperger, U.: Convective boundary layer evolution to 4 km asl over high-alpine terrain: Airborne lidar observations in the Alps, *Geophys. Res. Lett.*, 27(5), 689–692, 2000.

Putaud, J. P., Raes, F., Van Dingenen, R., Brüggemann, E., Facchini, M. C., Decesari, S., Fuzzi, S., Gehrig, R., Hüglin, C., Laj, P., Lorbeer, G., Maenhaut, W., Mihalopoulos, N., Müller, K., Querol, X., Rodriguez, S., Schneider, J., Spindler, G., ten Brink, H., Tørseth, K., and Wiedensohler, A.: European aerosol phenomenology-2: chemical characteristics of particulate matter at kerbside, urban, rural and background sites in Europe, *Atmos. Env.*, 38(16), 2579–2595, 2004.

Rader, D. J., and McMurry, P. H.: Application of the tandem differential mobility analyzer to studies of droplet growth or evaporation, *J. Aerosol Sci.*, 17(5), 771–787, 1986.

Randall, D. A., Wood, R. A., Bony, S., Colman, R., Fichet, T., Fyfe, J., Kattsov, V., Pitman, A., Shukla, J., Srinivasan, J., Stouffer, R. J., Sumi, A., and Taylor, K. E.: Contribution of Working Group I to the Fourth Assessment Report of the Intergovernmental Panel on Climate Change - Climate Models and their Evaluation, Cambridge University Press, Cambridge, United Kingdom and New York, 2007.

Sjogren, S., Gysel, M., Weingartner, E., Baltensperger, U., Cubison, M. J., Coe, H., Zardini, A. A., Marcolli, C., Krieger, U. K., and Peter, T.: Hygroscopic growth and water uptake kinetics of two-phase aerosol particles consisting of ammonium sulfate, adipic and humic acid mixtures,

**Hygroscopicity
Jungfrauoch,
Switzerland**

S. Sjogren et al.

Title Page

Abstract

Introduction

Conclusions

References

Tables

Figures

◀

▶

◀

▶

Back

Close

Full Screen / Esc

Printer-friendly Version

Interactive Discussion

**Hygroscopicity
Jungfraujoch,
Switzerland**

S. Sjogren et al.

Title Page

Abstract

Introduction

Conclusions

References

Tables

Figures

◀

▶

◀

▶

Back

Close

Full Screen / Esc

Printer-friendly Version

Interactive Discussion

J. Aerosol Sci., 38(2), 157–171, 2007.

Solomon, S., Qin, D., Manning, M., Alley, R. B., Bernsten, T., Bindoff, N. L., Chen, Z., Chidthaisong, A., Gregory, J. M., Hegerl, G. C., Heimann, M., Hewitson, B., Hoskins, B. J., Joos, F., Jouzel, J., Kattsov, V., Lohmann, U., Matsuno, T., Molina, M., Nicholls, N., Overpeck, J., Raga, G., Ramaswamy, V., Ren, J., Rusticucci, M., Somerville, R., Stocker, T. F., Whetton, P., Wood, R. A., and Wratt, D.: Contribution of Working Group I to the Fourth Assessment Report of the Intergovernmental Panel on Climate Change - Technical Summary, Cambridge University Press, Cambridge, United Kingdom and New York, 2007.

Stokes, R. H., and Robinson, R. A.: Interactions in aqueous nonelectrolyte solutions. I. Solute-solvent equilibria, J. Phys. Chem, 70, 2126–2130, 1966.

Swietlicki, E., Zhou, J. C., Covert, D. S., Hameri, K., Busch, B., Vakeva, M., Dusek, U., Berg, O. H., Wiedensohler, A., Aalto, P., Makela, J., Martinsson, B. G., Papaspiropoulos, G., Mentes, B., Frank, G., and Stratmann, F.: Hygroscopic properties of aerosol particles in the north-eastern Atlantic during ACE-2, Tellus, 52(2), 201–227, 2000.

Topping, D. O., McFiggans, G. B., and Coe, H.: A curved multi-component aerosol hygroscopicity model framework: Part 2 - Including organic compounds, Atmos. Chem. Phys., 5, 1223–1242, 2005a.

Topping, D. O., McFiggans, G. B., and Coe, H.: A curved multi-component aerosol hygroscopicity model framework: Part 1 - Inorganic compounds, Atmos. Chem. Phys., 5, 1205–1222, 2005b.

Verheggen, B., Cozic, J., Weingartner, E., Bower, K., Mertes, S., Connolly, P., Flynn, M., Gallagher, M., Choularton, T., and Baltensperger, U.: Aerosol partitioning between the interstitial and the condensed phase in mixed-phase clouds, J. Geophys. Res., doi:10.1029/2007JD008714R, 2007.

Vlasenko, A., Sjogren, S., Weingartner, E., Stemmler, K., Gäggeler, H. W., and Ammann, M.: Effect of humidity on nitric acid uptake to mineral dust aerosol particles, Atmos. Chem. Phys., 6, 2147–2160, 2006, <http://www.atmos-chem-phys.net/6/2147/2006/>.

Weingartner, E., Nyeki, S., and Baltensperger, U.: Seasonal and diurnal variation of aerosol size distributions ($10 < D < 750$ nm) at a high-alpine site (Jungfraujoch 3580 m a.s.l.), J. Geophys. Res., 104, (D21), 26 809–26 820, 1999.

Weingartner, E., Saathoff, H., Schnaiter, M., Streit, N., Bitnar, B., and Baltensperger, U.: Absorption of light by soot particles: determination of the absorption coefficient by means of aethalometers, J. Aerosol Sci., 34, (10), 1445–1463, 2003.

Weingartner, E., Gysel, M., and Baltensperger, U.: Hygroscopicity of aerosol particles at low temperatures. 1. New low-temperature H-TDMA instrument: Setup and first applications, *Environ. Sci. Technol.*, 36(1), 55–62, 2002.

5 Zelenyuk, A., Cai, Y., and Imre, D.: From agglomerates of spheres to irregularly shaped particles: Determination of dynamic shape factors from measurements of mobility and vacuum aerodynamic diameters, *Aerosol Sci. Technol.*, 40(3), 197–217, 2006.

10 Zhang, Q., Jimenez, J. L., Canagaratna, M. R., Allan, J. D., Coe, H., Ulbrich, I., Alfarra, M. R., Takami, A., Middlebrook, A. M., Sun, Y. L., Dzepina, K., Dunlea, E., Docherty, K., DeCarlo, P. F., Salcedo, D., Onasch, T., Jayne, J. T., Miyoshi, T., Shimojo, A., Hatakeyama, S., Takegawa, N., Kondo, Y., Schneider, J., Drewnick, F., Borrmann, S., Weimer, S., Demerjian, K., Williams, P., Bower, K., Bahreini, R., Cottrell, L., Griffin, R. J., Rautiainen, J., Sun, J. Y., Zhang, Y. M., and Worsnop, D. R.: Ubiquity and dominance of oxygenated species in organic aerosols in anthropogenically-influenced Northern Hemisphere midlatitudes, *Geophys. Res. Lett.*, 34(13), 2007.

**Hygroscopicity
Jungfraujoch,
Switzerland**

S. Sjogren et al.

Title Page

Abstract

Introduction

Conclusions

References

Tables

Figures

◀

▶

◀

▶

Back

Close

Full Screen / Esc

Printer-friendly Version

Interactive Discussion

Hygroscopicity Jungfraujoch, Switzerland

S. Sjogren et al.

Table 1. Overview of the campaigns.

		Dry diameter, D_0 [nm]		
		50	100	250
2000 – Winter				
Date	21.02 to 27.03.2000			
Number of scans* at constant RH		1698	1855	1648
Number of humidograms		11	15	11
T setting HTDMA, inlet type	–10°C, interstitial, PM1			
2002 – Summer				
Date	08.07 to 17.07.2002			
Number of scans* at constant RH		528	746	517
Number of humidograms		4	43	4
T setting HTDMA, inlet type	0.5°C, interstitial, PM1			
2004 – Winter				
Date	01.03 to 01.04.2004			
Number of scans* at constant RH		499	1767	1295
Number of humidograms		4	4	4
T setting HTDMA, inlet type	–10°C (as well as shortly 20°C), interstitial, PM2.5			
2005 – Spring-like				
Date	13.02 to 16.03.2005			
Number of scans* at constant RH		306	1533	162
Number of humidograms		6	6	6
T setting HTDMA, inlet type	25°C, total inlet			

*Each scan had a duration of 300 s.

Title Page	
Abstract	Introduction
Conclusions	References
Tables	Figures
◀	▶
◀	▶
Back	Close
Full Screen / Esc	
Printer-friendly Version	
Interactive Discussion	

Hygroscopicity Jungfraujoch, Switzerland

S. Sjogren et al.

Table 2. Hygroscopic growth factors for pure substances and physical properties used (Bulk properties, Topping et al., 2005a).

Substance	GF (at $a_w = 0.85$)	Density [kg m^{-3}]
$(\text{NH}_4)_2\text{SO}_4$	1.56	1769
NH_4HSO_4	1.62	1780
NH_4NO_3	1.59	1720
H_2SO_4	1.88	1830
BC	1.0	2000
Organics	1.20 ^a	1400 ^b

^a The growth factor of the organics was chosen to give a best fit between measurement and model. This value is in accordance with the GF measured for secondary organic aerosol (SOA) (Duplissy et al., 2007³; Baltensperger et al., 2005).

^b The density of organics was chosen to represent oxidized organics in aged atmospheric aerosol (Alfarra et al., 2006; Dinar et al., 2006).

[Title Page](#)
[Abstract](#)
[Introduction](#)
[Conclusions](#)
[References](#)
[Tables](#)
[Figures](#)
[Back](#)
[Close](#)
[Full Screen / Esc](#)
[Printer-friendly Version](#)
[Interactive Discussion](#)

Hygroscopicity Jungfrauoch, Switzerland

S. Sjogren et al.

Table 3. Summary of averages of GF and average spread σ of the GF distributions for the campaigns.

Campaign date Season	Feb–Mar 2000			July 2002			Mar 2004			Feb–Mar 2005		
	Winter			Summer			Winter			Spring-like		
Dry diameter D_0 [nm]	50	100	250	50	100	250	50	100	250	50	100	250
Average GF^* at 85% RH	1.33	1.40	1.41	1.26	1.29	1.35	1.34	1.40	1.47	1.30	1.35	1.42
-Std.dev. of GF^*	0.091	0.104	0.133	0.090	0.076	0.081	0.122	0.112	0.114	0.081	0.076	0.076
Number of scans	1698	1855	851	528	746	517	499	1767	1295	306	1533	162
Spread σ	0.13	0.15	0.19	0.08	0.10	0.12	0.11	0.13	0.15	0.17	0.16	0.16
-Std.dev. of σ	0.041	0.046	0.070	0.045	0.043	0.043	0.050	0.055	0.063	0.095	0.058	0.089
Mean GF^* at 85% RH	1.34	1.41	1.44	1.25	1.29	1.36	1.33	1.41	1.48	1.31	1.34	1.41

Title Page

Abstract

Introduction

Conclusions

References

Tables

Figures

◀

▶

◀

▶

Back

Close

Full Screen / Esc

Printer-friendly Version

Interactive Discussion

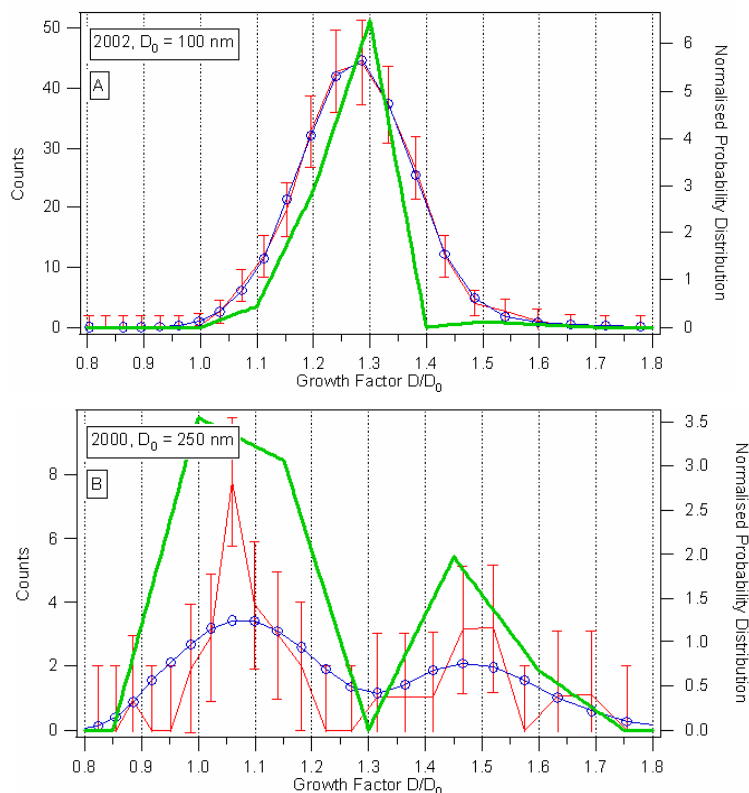


Fig. 1. Typical examples of growth factor distributions of $D_0=100$ nm particles ($GF=1.28$) and $\sigma=0.08$ (Panel (A), 12 July 2002 18:00) and of $D_0=250$ nm particles during a SDE (Panel (B), 17 March 2000 20:24), with a first mode at $GF=1.05$ and a second mode at $GF=1.45$ (overall $\sigma=0.22$). The red line and points (left axis) refer to measured particle counts, the green line is the inverted GF distribution (right axis) and the blue line inverted growth distribution reprocessed through the forward model (left axis). Error bars indicate the estimated counting uncertainty of the measurement.

[Title Page](#)
[Abstract](#)
[Introduction](#)
[Conclusions](#)
[References](#)
[Tables](#)
[Figures](#)
[◀](#)
[▶](#)
[◀](#)
[▶](#)
[Back](#)
[Close](#)
[Full Screen / Esc](#)
[Printer-friendly Version](#)
[Interactive Discussion](#)

**Hygroscopicity
Jungfrauoch,
Switzerland**

S. Sjogren et al.

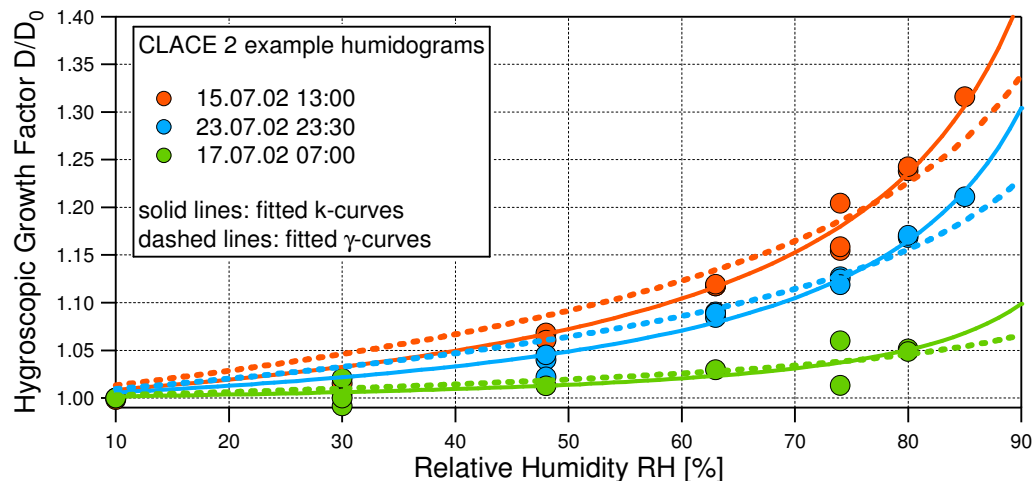


Fig. 2. Typical humidograms of particles with $D_0=100$ nm sized particles during July 2002 (the other campaigns gave similar results). The hygroscopicity at the JFJ varies with varying season and origin of air parcels, but the water uptake at a specific time can be well described as a function of RH with a single-parameter model (solid lines).

Title Page

Abstract

Introduction

Conclusions

References

Tables

Figures

◀

▶

◀

▶

Back

Close

Full Screen / Esc

Printer-friendly Version

Interactive Discussion

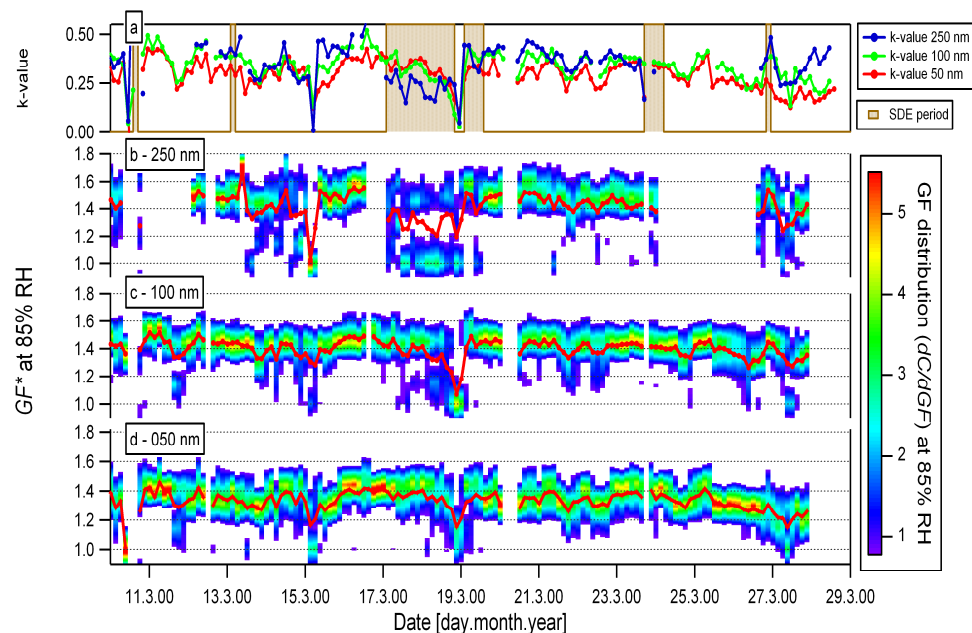


Fig. 3. Temporal evolution of GF distributions for GF all measured sizes ($D_0=50, 100, 250$ nm) at $RH=85\%$, during year 2000. Panel (a) shows the k -values indicating the hygroscopicity of the aerosol. The red lines on panels (b), (c) and d represent the ensemble mean growth factor GF^* .

[Title Page](#)
[Abstract](#)
[Introduction](#)
[Conclusions](#)
[References](#)
[Tables](#)
[Figures](#)
[◀](#)
[▶](#)
[◀](#)
[▶](#)
[Back](#)
[Close](#)
[Full Screen / Esc](#)
[Printer-friendly Version](#)
[Interactive Discussion](#)

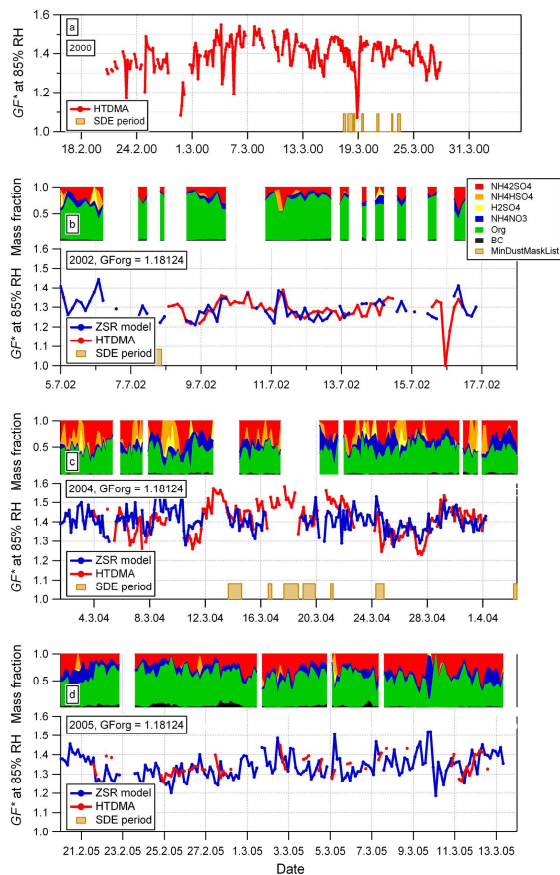


Fig. 4. Time series of the GF^* for $D_0=100$ nm particles at the JFJ for each campaign measured (each lower panel), as well as the chemical composition (each top panel). The predicted GF^* from composition data is shown as the blue line in the GF panels and the measured in red. During winter 2000 no high time resolution composition data were available.

[Title Page](#)
[Abstract](#)
[Introduction](#)
[Conclusions](#)
[References](#)
[Tables](#)
[Figures](#)
[Back](#)
[Close](#)
[Full Screen / Esc](#)
[Printer-friendly Version](#)
[Interactive Discussion](#)

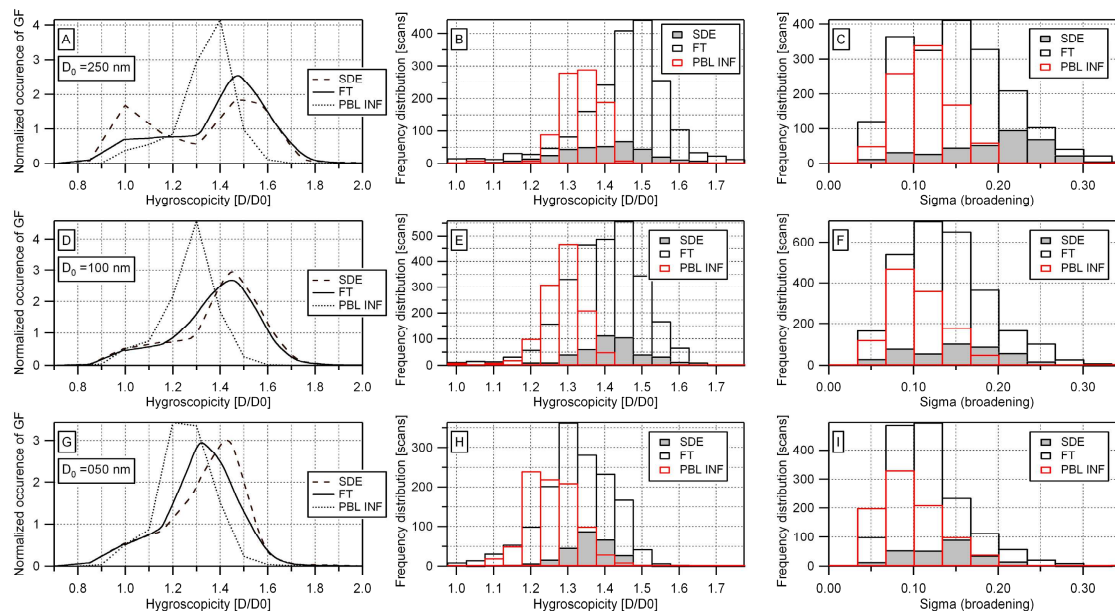


Fig. 5. From top row to bottom, the dry sizes $D_0=250$, 100, 50 nm are presented. First column shows the GF distribution for SDE, FT and PBL INF conditions. Second column shows the frequency distribution of GF^* . Third column shows the frequency distribution of the spread σ , a measure for the broadening of the GF distribution.

[Title Page](#)
[Abstract](#)
[Introduction](#)
[Conclusions](#)
[References](#)
[Tables](#)
[Figures](#)
[⏪](#)
[⏩](#)
[◀](#)
[▶](#)
[Back](#)
[Close](#)
[Full Screen / Esc](#)
[Printer-friendly Version](#)
[Interactive Discussion](#)